OPTIMIZING TRENCHING DEVICE OPERATIONAL PARAMETERS VIA MBD-DEM COUPLING FOR ENERGY SAVINGS

/

基于MBD-DEM耦合法优化开沟装备作业参数以减少能源消耗

Haochao TAN, Congcong SHEN, Junlong MA, Chunlin WU, Liming XU, Shuai MA*) [1]
College of Engineering, China Agricultural University, Beijing 100083 / China
Tel: +86- 17710628251; E-mail: mashuaicoe@cau.edu.cn
Corresponding author: Shuai MA
DOI: https://doi.org/10.35633/inmateh-74-83

Keywords: *trenching device; operational parameter; MBD-DEM; energy saving*

ABSTRACT

This study addresses the challenges of high resistance, energy consumption, and complex operations in deep trenching in orchards by proposing a reverse trenching and backfilling scheme. A reverse-rotating chain trencher was designed for integrated trenching and backfilling. Through mechanical analysis and MBD-DEM coupled simulation, operating parameters affecting the process were identified. A three-factor, three-level test with forward speed (v), rotation speed (n), and working angle (γ) determined the optimal parameters as v=0.29 km/h, n=393 r/min, γ=15°. Field tests yielded specific energy consumption of 0.328 kWh m^{-3} and mean torque of 416.66 Nm, with simulation errors of 2.18% and 4.03%, respectively.

摘要

本研究针对果园深开沟作业中存在的阻力大、能耗高及作业复杂等问题，提出了反向开沟与回填作业方式，设计了反向旋转链式开沟回填一体机。通过力学分析与 MBD-DEM 联合仿真，明确了影响该作业方式运行的主要参数。通过三因素三水平正交试验确定了前进速度（v）、刀轴转速（n）和工作角度（γ）的最佳参数组合为 v=0.29 km/h、n=393 r/min、γ=15°。田间试验得到的比能耗为 0.328 kW·h m^{-3}，平均扭矩为 416.66 Nm，仿真误差分别为 2.18%和 4.03%。

INTROUCTION

Trenching and fertilizing are critical aspects of orchard management, particularly for deep trenching operations, which aid in promoting root growth, enhancing water retention capabilities, and improving nutrient distribution efficiency. Currently, the commonly used disc trenching machines primarily focus on a trenching depth of approximately 45 cm, but this depth often comes with high energy consumption issues. Therefore, reducing the resistance and energy consumption during the trenching process has become a key focus for agricultural experts *(Chen et al., 2024; Liu et al., 2022; Yang et al., 2023)*. *Liu et al., (2024),* analyzed the power consumption of the counter-rotating trenching machine's cutter roll, explored the power consumption and resistance of the cutter roll under different soil particle diameters, and provided reference for the cutter roll-soil coarse-grained model. *Zeng et al., (2024),* addressed the issue of high-power consumption in blade trenching by designing a layered cutting and throwing trenching blade set. They optimized the working parameters of the trenching blade and conducted field tests, showing that the specific energy consumption of the optimized blade set was reduced by 8.31%. *Liu et al., (2023),* designed a counter-rotating twin-shaft spiral trenching machine. They analyzed the effects of different working parameters on the trenching performance and power consumption of the cutting knife. After optimizing the operating parameters of the trenching machine, they conducted field tests with the optimal parameters, obtaining a trenching qualification rate of 91.4% and an average soil crushing rate of 72%. *Wang et al., (2024),* studied the effects of forward speed, blade trenching angle, and width on trenching resistance based on the discrete element method, optimized the optimal parameters, and found that the minimum trenching resistance was 58.54 N under the optimized parameters, with an error of less than 10% between simulation and experimental values.

[1] *Haochao Tan, Ph.D.; Congcong Shen, Ph.D.; Junlong Ma, Ph.D.; Chunlin Wu, Ms.; Liming Xu, professor, Ph.D.; Shuai Ma, associate professor Ph.D.*

Although the aforementioned scholars have optimized the parameters of trenching machines through a combination of numerical simulation and field tests, reducing operational energy consumption, the depth of these trenching machines is generally shallow and unable to meet the 60 cm trenching depth required for deep-rooted crops like grapes.

While chain trenching machines can achieve trenching up to 100 cm, they have high resistance and energy consumption and are relatively complex to operate. Therefore, to address these issues, this paper proposes a chain counter-rotating trenching solution that simultaneously accomplishes trenching and backfilling. The feasibility of this solution has been demonstrated through MBD-DEM coupled simulation, and on this basis, operational parameters of the trenching machine have been optimized to reduce working energy consumption, with the optimization results validated through field tests.

MATERIAL AND RESEARCH METHODS

Structure and working principle

Traditional chain trenchers (hereinafter referred to as traditional trenchers) rotate in a forward direction, piling soil in front of the implement and forcing the accumulated soil to the sides through a spiral soil-separating wheel (Fig.1a). Subsequent backfilling is required to return the soil to the trench, making the process cumbersome. To achieve simultaneous trenching and backfilling, this paper proposes a reverse-rotating chain trencher (hereinafter referred to as reverse trencher) (Fig.1b). This device attempts to throw soil back into the trench by reversing the rotation of the trenching chain, thereby achieving the simultaneous process of trenching and backfilling. The device does not leave deep trenches on the ground surface after completing its operation. The specific backfilling effect of this innovative idea still requires subsequent simulation verification to confirm its feasibility.

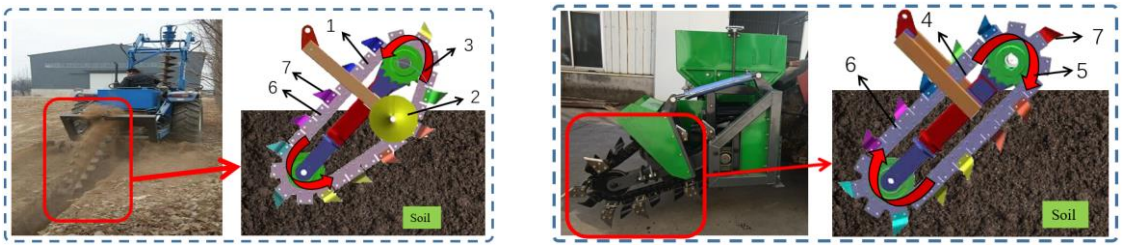

a) Traditional trencher *b) Reverse trencher*

Fig. 1 - Trencher comparison

1- Traditional chain trencher; 2- Spiral soil separator wheel; 3- Forward rotation; 4- Reverse trencher; 5- Reverse rotation; 6- Trenching chain;7-Trenching blade

Force analysis during the soil cutting process

To reduce the energy consumption of the reverse trencher, it is necessary to determine the operational parameters affecting soil cutting through mechanical analysis of the operation process. The main stages of reverse trench operation include: cutting stage (oc), convert stage (cd), soil lifting stage (da), and idling stage (ao) (Fig.2). The main force-bearing stages are the cutting stage and the soil lifting stage, so analysis of these two stages is required.

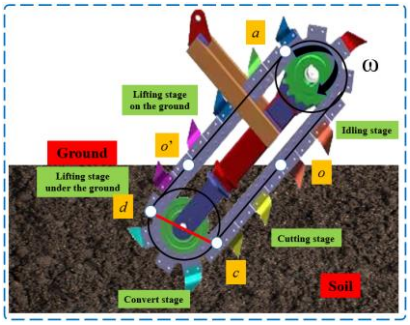

Fig. 2- Schematic diagram of the operating stage of the reverse trencher

Mechanical analysis of the cutting stage

According to Fig. 2, during the cutting stage, the trenching blade operates at a certain angle with the ground. Therefore, the force analysis will be based on the normal working state. The force analysis is shown in Fig. 3. On the cutting surface, the Y-axis is parallel to the positive cutting edge of the trenching blade, the Z-axis is perpendicular to the positive cutting edge and points upward, and the X-axis is perpendicular to cutting surface.

Thus, a coordinate system XYZ is established, wherein the advantage of this coordinate system is that most of the forces lie on the coordinate axes. Taking the forward direction as Y'-axis, the direction perpendicular to the ground and upward as Z'-axis, and the direction perpendicular to the forward direction as the X'-axis, a coordinate system X'Y'Z' is established. The purpose of this coordinate system is to ensure that the gravity of the soil block is parallel to the Z'-axis, facilitating subsequent decomposition.

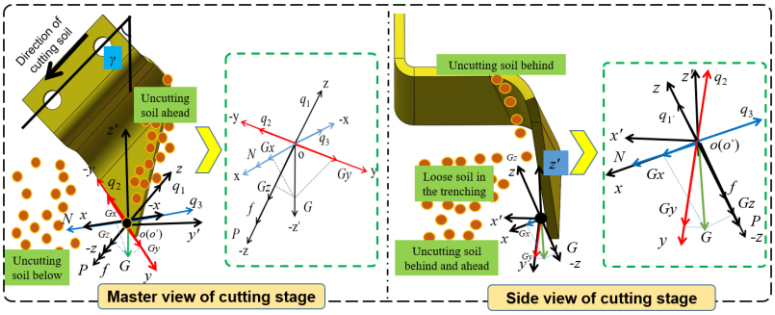

Fig. 3- Mechanical analysis of the soil cutting stage

In the diagram, *-x*, *-y*, *-z*, and *-z'* represent the negative directions of the *x*, *y*, *z*, and *-z'* axes, respectively, while *o* and *o'* represent the origins of the coordinate systems *xyz* and *x'y'z'*, respectively. With this understanding, the force equation for the cutting stage is established as follows:

$$\begin{cases} \sum F_x = G_x + N - q_3 \\ \sum F_y = G_y - q_2 \\ \sum F_z = q_1 - G_z - f - P \end{cases} \tag{1}$$

where: N represents the support force of the trenching blade on the soil, P represents the cutting force of the blade on the soil, q_1 represents the resistance of the uncut soil below, q_2 represents the resistance of the uncut soil in front, q_3 represents the resistance exerted by the loose soil inside the furrow, f represents the frictional force of the soil on the blade during motion, F_x, F_y and F_z represent the total forces experienced along the *x*, *y* and *z* axes respectively, G_x, G_y and G_z represent the components of force G along the *x*, *y* and *z* axes. These components are related to the structure parameters of the trenching blade, specifically the bending line inclination angle and the curvature，as shown in equation (2) and (3):

$$\begin{cases} G_x = G\left(\sin\beta\sin\gamma - \sin\alpha\cos\beta\cos\gamma\right) \\ G_y = -G\left[\sin\gamma\left(\cos^2\alpha\sin\beta + \sin^2\alpha\cos\beta\right) + \sin\alpha\sin\beta\cos\gamma\right] \\ G_z = -G\left[\cos\alpha\cos\gamma - \sin\gamma\sin\alpha\cos\beta\left(\cos\alpha\sin\beta + \sin\alpha\right)\right] \end{cases} \tag{2}$$

$$f = \mu N = \mu N_L\left[dL\cos\alpha + d^2L^2\left(1-\tan\theta\right)\right] \tag{3}$$

where, G represents the weight of the soil being cut, μ represents the friction coefficient, θ represents the cone residual angle, which affects the size of the cutting surface of the trenching blade. N_L represents the support force on the unit cutting surface area. α and β denote the bending line angle and curvature of the trenching blade *(Tan et al., 2024)*, while γ represents the working angle of the reverse trencher.

From (1)~(3), it can be seen that the main factors affecting soil cutting resistance are the gravity (G) of the soil block, the cone residual angle (θ), curvature (β), and bending line angle (α). Among them, the gravity (G) is related to the forward speed (v) and rotational speed (n). The faster the forward speed, the greater the length of the soil block in the Y'-direction per unit time. Similarly, the faster the chain rotation speed, the greater the length of the soil block in the Z'-direction per unit time, resulting in a greater gravity of the soil block. Therefore, the gravity can be determined by the forward speed (v) and rotational speed (n).

Mechanical analysis of the soil lifting stage

In Fig. 4, -x' and -y' represent the negative directions of the x' and y' axes, respectively. In this stage, including the above-ground soil lifting and the underground soil lifting, the focus will be on analyzing the complex force distribution in the underground soil lifting section. Some of the soil will move along with the movement of the trenching blades. The force analysis is shown in Fig. 4, and the force equations are as follows:

$$\begin{cases} \sum F_{x'} = -q_{x'y'}\cos\theta_5 + N_{x'y'}\cos\theta_4 - f_{x'y'}\cos\theta_6 \\ \sum F_{y'} = -q_{z'y'}\cos\theta_1 + N_{z'y'}\cos\theta_2 + f_{z'y'}\cos\theta_3 \\ \sum F_{z'} = -G - q_{z'y'}\sin\theta_1 + N_{z'y'}\sin\theta_2 + f_{z'y'}\sin\theta_3 \end{cases} \quad (4)$$

where, $q_{x'y'}$, $f_{x'y'}$, and $N_{x'y'}$ represent the projections of q_2, f, and N on the X'O'Y' plane. $q_{z'y'}$, $f_{z'y'}$, and $N_{z'y'}$ represent the projections of q_2, f, and N on the Z'O'Y' plane. θ_1 to θ_6 represent the angles between the projection forces and the coordinate axes. The presence of $N_{z'y'}\sin\theta_2$ and $f_{z'y'}\sin\theta_3$ forces allows the soil to lift off the ground and move upward. The presence of $N_{z'y'}\cos\theta_2$ and $f_{z'y'}\cos\theta_3$ forces causes the lifted soil to move along the direction of the trencher operation. Therefore, in the Y'O'Z' plane, the motion of the soil is a combined motion in the forward direction and vertically upward, and the trajectory of the motion approximates that of the trenching blades. At this stage, the values of θ_1 to θ_6 are determined by the working state of the blades, and they remain constant as long as the working state remains unchanged. The working state of the blades is determined by three factors: α, β, and γ, so the influencing factors of this stage can still be considered to be determined by α, β, and γ.

Based on our analysis, key trenching parameters were identified as α, β, γ, R, θ, n, and v. In previous work, the structural parameters α, β, R, and θ were optimized, enhancing blade performance. Now, the aim is to optimize the operational parameters γ, n, and v to reduce energy consumption and find the optimal combination.

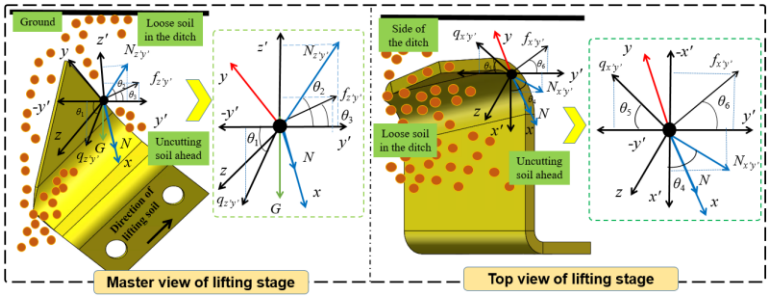

Fig. 4 - Mechanical analysis of the soil lifting stage

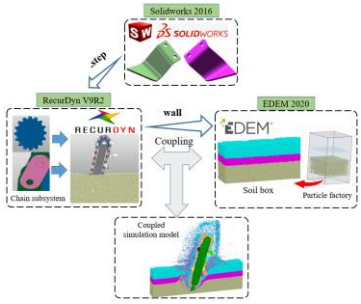

Fig. 5 - Schematic diagram of simulation model building

The establishment of a simulation model

In this study, the bidirectional MBD-DEM coupling method is employed to optimize the operating parameters. The soil is considered as discrete element particles *(Kešner et al., 2021; Tamás & Bernon, 2021; Wang et al., 2020)*, and the size of soil particles is simplified, setting the diameter of soil particles to 5 mm *(Wang et al., 2023)*. A Hysteretic Spring model and Linear Cohesion model were used as the contact models between particles *(Ma et al., 2021)*. A soil-box model was built with dimensions of 4000 mm in length, 600 mm in width, and 650 mm in height. First, the forward and reverse rotation of the trencher chain in RecurDyn are set. This is to analyze the feasibility of real-time soil backfilling by the reverse trencher. The simulation runs for 7 seconds, saving data every 0.2 seconds. Based on the feasibility, the operating parameters are optimized to reduce the reverse trencher energy consumption. In this study, 3D models of the trenching blade were designed using SolidWorks and were saved in "Step" format. These models were then imported into the RecurDyn interface. The “chain” command in RecurDyn software was utilized to establish a chain drive system. Based on the operational requirements, rotational and translational joints and driving speeds were set for the chain, and the dynamic system was exported to EDEM software in “.wall” format. The complete simulation model and process are shown in Fig. 5, the discrete element parameters were determined as shown in Table 1 *(Tan et al., 2024)*.

Table 1

Parameters of discrete element simulation

Type	Static friction coefficient	Rolling friction coefficient	Restitution coefficient	Adhesive energy density / (J m^{-3})
Upper soil	0.6	0.07	0.47	2694
Middle soil	0.5	0.17	0.52	4266
Lower soil	0.5	0.21	0.62	4432
65Mn- Upper soil	0.72	0.33	0.44	-
65Mn- Middle soil	0.8	0.16	0.54	-
65Mn- Lower soil	0.7	0.32	0.51	-

Experimental design

A simulation test with three factors (operating speed v=0.2, 0.4, and 0.6 km/h, rotational speeds n=200, 300, and 400 r/min, and working angles γ=15°, 25°, and 35°) and three levels was conducted, using the mean driving torque (T) of the reverse trencher and the specific energy consumption (Q) as evaluation indicators. 17 simulation experiments (Box-Behnken Design) were designed, including 5 repeats, with factors and results shown in Table 2. Among them, the calculation formula for specific energy consumption is shown as Equation 5.

$$Q = \frac{Tn}{9550vks} \quad (5)$$

where, Q represents specific energy consumption (kWh m^{-3}); T represents mean torque (Nm); n represents rotational speed (r min^{-1}); v represents forward speed (m/h); P represents the driving power (kW); k represents the trench width (mm); s represents the trench depth (mm).

Table 2

The experimental factors and level designs

No.	Actual factor level			Coded factor level			Results	
	Forward speed v (km h^{-1})	Rotational speed n (r min^{-1})	Working angle γ (°)	Forward speed v (km h^{-1})	Rotational speed n (r min^{-1})	Working angle γ (°)	Mean torque T (Nm)	Specific energy consumption Q (kWh m^{-3})
1	0.2	200	25	-1	-1	0	1006	0.585
2	0.6	400	25	1	1	0	433.95	0.168
3	0.4	400	15	0	1	-1	334.17	0.194
4	0.4	400	35	0	1	1	428.2	0.249
5	0.6	300	35	1	0	1	433.37	0.126
6	0.2	300	35	-1	0	1	381.68	0.333
7	0.4	200	15	0	-1	-1	887.72	0.258
8	0.6	200	25	1	-1	0	992.56	0.192
9	0.4	200	35	0	-1	1	730.84	0.212
10	0.6	300	15	1	0	-1	690.39	0.201
11	0.2	300	15	-1	0	-1	631.57	0.551
12	0.2	400	25	-1	1	0	390.68	0.455
13	0.4	300	25	0	0	0	557	0.218

RESULTS

Reverse trencher feasibility analysis

To verify the feasibility of the proposed reverse trencher, simulations for both forward and reverse rotations were conducted. Based on the simulation model built in Fig. 5, the sprockets were set to rotate forward and backward at a speed of 250 r/min, with a forward speed of 1 km/h. To observe the movement of soil particles under these two motion modes, a region with dimensions of 300 mm in length, width, and height was selected at the midpoint of the simulation time, as shown in Fig. 6. Analysis was conducted for the time period from 3.8 to 4.6 s, as during this time interval, the trenching device passes through this area precisely.

According to Fig. 6, soil particles near the trenching blade have higher movement speeds, while those further away have lower speeds, indicating that the trenching blade is the main cause of soil movement. From Fig. 6(a), it can be seen that in the forward rotation mode, soil particles move upward and forward along with the trenching blade. At 4.4 seconds, some soil particles continue moving with the trenching blade, while others accumulate forward due to the obstruction of the shell; at 4.6 seconds, a small amount of soil entering the shell moves to the rear of the trenching device and backfills into the trench, while most soil particles continue to accumulate forward, as shown in Fig. 6(c). Continuous soil accumulation obstructs the forward movement of the trenching device, increasing the trenching resistance. Therefore, this traditional forward rotation trenching device usually needs to be equipped with a spiral conveyor structure to continuously transport accumulated soil to the sides of the trench, clearing the soil ahead. From Fig. 6(b), it can be seen that soil particles in the designated area move downward and backward with the trenching blade, and at 4.6 seconds, almost all soil is thrown to the rear, as shown in Fig. 6(d). In the reverse trenching mode, soil ahead of the trenching device is not accumulated but directly thrown backward. Although some soil may enter behind the shell under the action of the trenching blade, it eventually backfills into the trench due to collision with the shell, resulting in almost no change in soil height inside the trench.

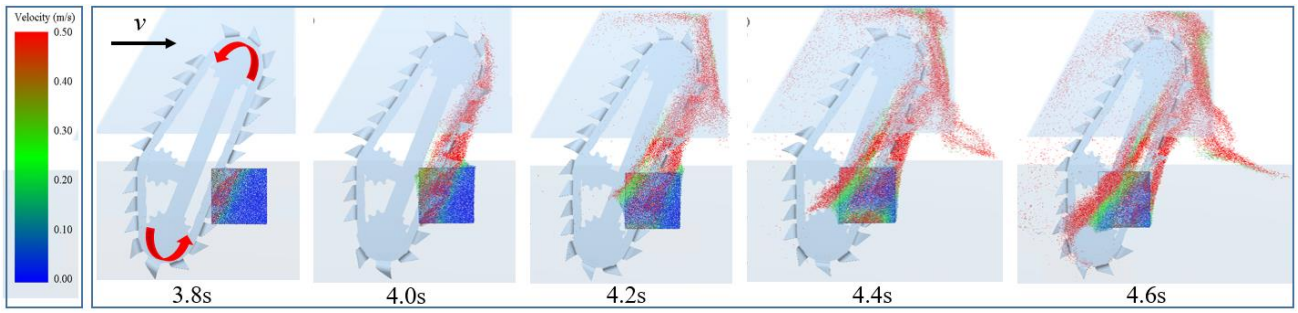

a) Soil movement situation under forward mode

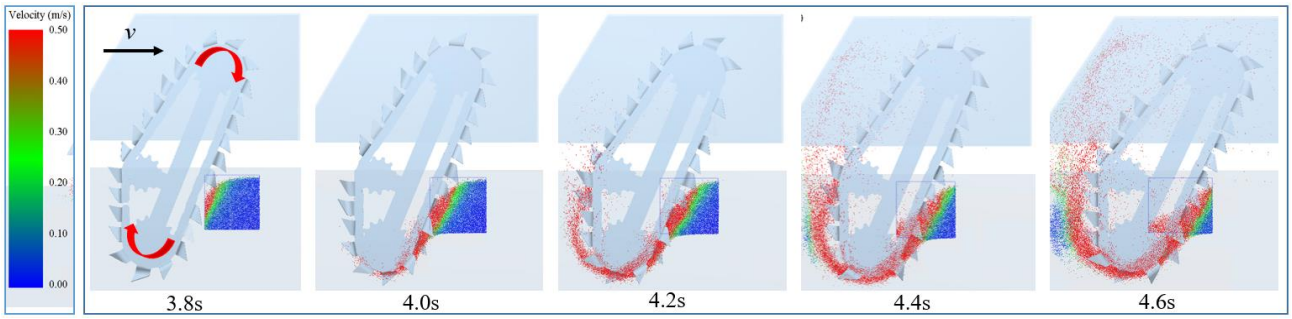

b) Soil movement situation under reverse mode

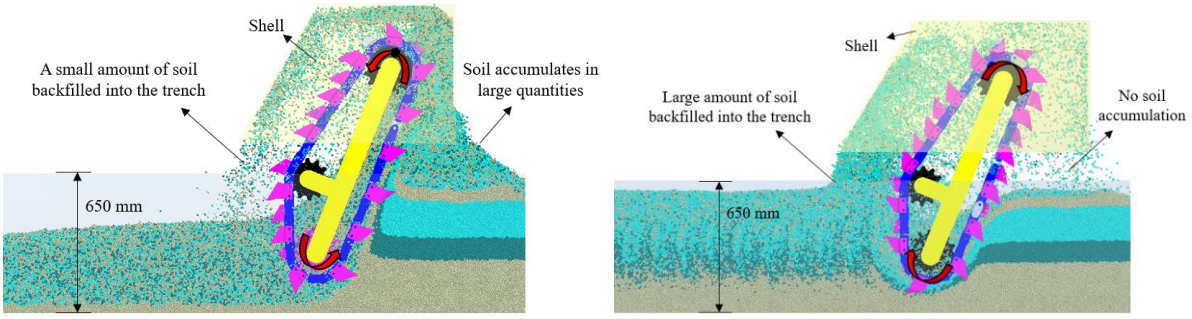

c) Simulation results under forward mode *d) Simulation results under reverse mode*

Fig. 6 - Soil movement trajectory

Particle Motion Velocity Analysis

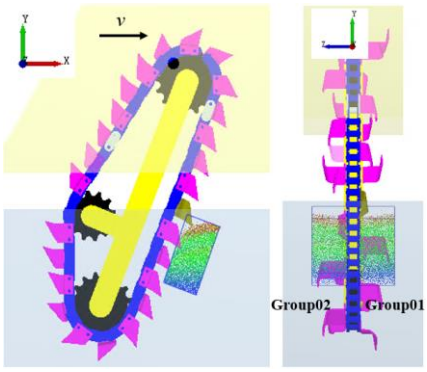

Fig. 7 - Schematic diagram of the selected area

In order to further illustrate the feasibility of verifying the reversed trenching, two Groups with length, width, and height of 150, 300, and 150 mm were set up, respectively. The Groups are parallel to the chain in the XOY plane, and are located on the left and right side of the trench in the ZOY plane, respectively. They are named as Group01 and Group02, respectively, as shown in Fig. 7, which are used to react to the movement pattern of soil particles on both sides.

The time period during which the trenching blades exactly pass through this position is from 3.8 to 4.4 seconds. The average motion speeds of particles in the XYZ directions for two groups (Group01 and Group02) within this time period are shown in Fig. 8. From Fig. 8(a) ~ (c), it can be seen that within Group01, the magnitudes of speeds in the XYZ axes under both forward and reverse rotation modes are basically the same, but the directions are completely opposite.

In the forward rotation mode, the speeds in the XY axes are positive, indicating that the soil particles have a tendency to move forward and upward. In the reverse rotation mode, the speeds are negative, indicating that the soil moves downward and backward, which is consistent with the motion trajectory described in Fig. 6. In the forward rotation, negative Z-axis speed indicates soil particles spread outward from the ditch, throwing some soil to the left. In reverse rotation, positive Z-axis speed signifies soil particles converge inward into the ditch, transporting soil into it. Since Group01 and Group02 are located in symmetric positions, the trend of soil particle speed changes in Group02 is generally consistent with that in Group01 (Fig. 8(d) and (f)), but the magnitudes are slightly different. The difference is that along the Z-axis, in forward rotation, the speed is positive, indicating a tendency for soil particles to be thrown to the other side of the ditch, while in reverse rotation, the speed is negative, indicating a tendency for soil particles to converge inward towards the ditch under the influence of the trenching blade.

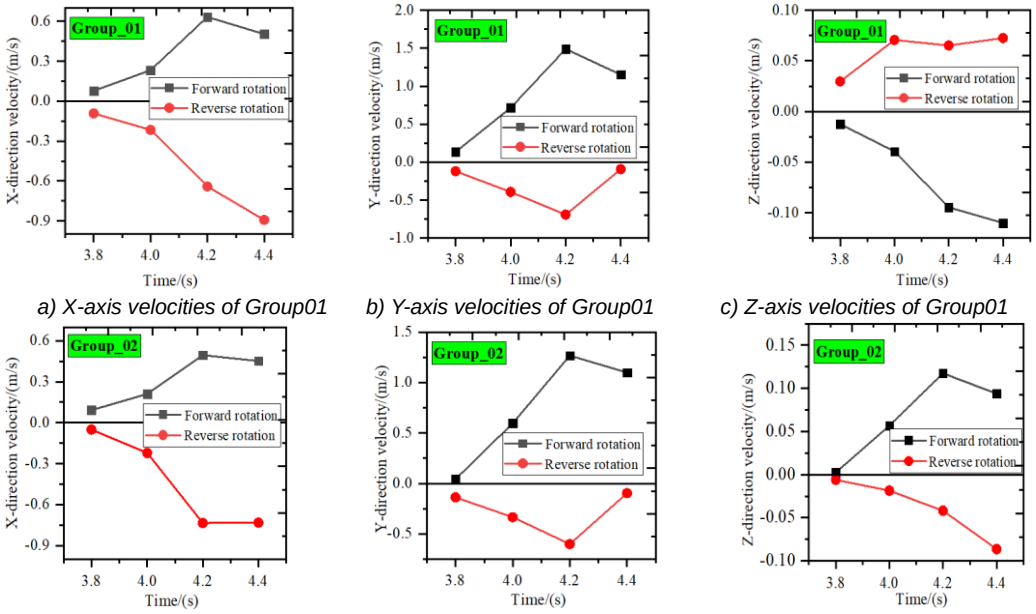

a) X-axis velocities of Group01 *b) Y-axis velocities of Group01* *c) Z-axis velocities of Group01*

d) X-axis velocities of Group02 *e) Y-axis velocities of Group02* *f) Z-axis velocities of Group02*

Fig. 8 - Velocity analysis of soil particles

Based on the analysis of soil particle motion speeds described above, the distribution of soil particles along the Z-axis at 4.4 seconds is observed (Fig. 9). From the figure, the position distribution of soil particles can be visually observed. In the same coordinate system, during forward rotation, the particle positions in the two groups are opposite: Group01 is mainly negative, and Group02 is mainly positive, indicating soil spreading outward. During reverse rotation, soil particles in both groups converge towards the center, facilitating easier backfilling of soil into the furrow. Based on the above analysis, this study proposes for the first time that the reverse trencher can meet the soil backfilling requirements. The reverse rotation mode is feasible, and subsequent field trials will be conducted using this new operational method.

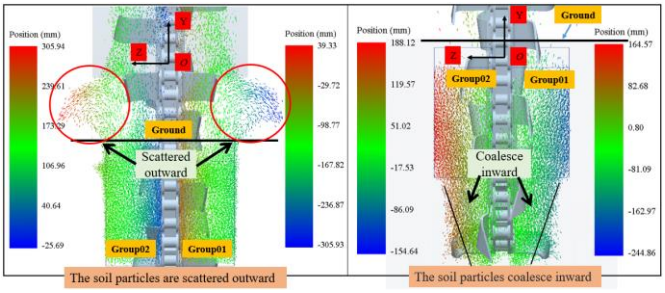

a) Forward Rotation *b) Reverse Rotation*

Fig. 9 - Distribution angle of Soil Particles along the Z-axis

Analysis of significance

Based on the results in Table 2, an analysis of variance (ANOVA) was conducted on the experimental factors, with the results shown in Table 3. Among the single factors, forward speed has a significant impact on energy consumption, and rotation speed has a significant impact on the mean torque.

Among the interaction terms, the interaction between rotation speed and working angle significantly impacts energy consumption, and the interaction between forward speed and working angle significantly impacts the mean torque. The impact of other factors is not significant. The regression equations for the response values can be expressed as Equation (6) and (7):

$$Q = 0.26 - 0.15v - 0.023n + 0.00267\gamma + 0.027vn + 0.036v\gamma + 0.025n\gamma + 0.087v^2 - 0.035\gamma^2 - 0.075v^2\gamma \quad (6)$$

$$T = 600.59 + 17.54v - 253.77n - 15.71\gamma + 14.18vn + 62.73n\gamma + 90.46n^2 - 81.08\gamma^2 - 111.02v^2\gamma \quad (7)$$

Table 3

The ANOVA of specific energy consumption and mean torque

Dependent variable	Source of variance	Sum of square	Degree of freedom	*F* value	*P* value
Q	*v*	0.19	1	207.46	< 0.0001**
	n	4.147e^{-3}	1	4.50	0.0715
	γ	2.056e^{-5}	1	0.022	0.8854
	vn	2.836e^{-3}	1	3.08	0.1227
	nγ	5.133e^{-3}	1	5.57	0.050
	n^2	2.517e^{-3}	1	2.73	0.1423
	γ^2	0.032	1	34.57	0.0006**
	$v^2\gamma$	5.093e^{-3}	1	5.53	0.0510
T	*v*	2461.91	1	0.95	0.3589
	n	515200	1	198.28	< 0.0001**
	γ	987.53	1	0.38	0.5547
	vn	804.01	1	0.31	0.5932
	vγ	15738.96	1	6.06	0.0392**
	v^2	34552.7	1	13.30	0.0065**
	γ^2	27758.19	1	10.68	0.0114**
	$v^2\gamma$	24648.66	1	9.49	0.0151**

Interaction analysis

In order to further analyze the effects of various factors on torque and specific energy consumption, an interaction analysis was conducted. One factor is fixed at a 0 level and the effects of remaining two factors on Q and T is observed. From Fig. 10(a), it is evident that as rotational speed (*n*) and forward speed (*v*) increase, Q gradually decreases. When *n* is fixed at a certain level, Q increases rapidly with a decrease in *v*, showing a steep slope in response surface along the *v* direction. When *v* is fixed at a certain level, Q decreases with an increase in *n*, and when *v* is at a lower level, the increase in *n* has a minimal effect on Q. This indicates that the interaction between *n* and *v* has a non-significant impact on Q. The same trend can be observed from Fig. 10(b), where Q decreases with an increase in *v* and working angle (γ), but the magnitude of change is small, suggesting a weak interaction effect between the two factors.

From Fig. 10(c), it can be seen that T increases with an increase in *v* and a decrease in *n*. Regardless of the level at which *n* is fixed, T remains relatively stable with changes in *v*. Similarly, regardless of the level at which *v* is fixed, T remains stable with changes in *n*. This indicates that the interaction between *n* and *v* does not significantly affect T. This is consistent with the results reflected in Table 3. Conversely, from Fig. 10(d), when *n* is at a lower level, T decreases with an increase in γ. However, when *n* is at a higher level, T increases with an increase in γ. This suggests that the presence of *n* changes the impact of γ on T, indicating a significant interaction effect between *n* and γ. Therefore, to reduce T, consider a higher value of *n* and a smaller value of γ.

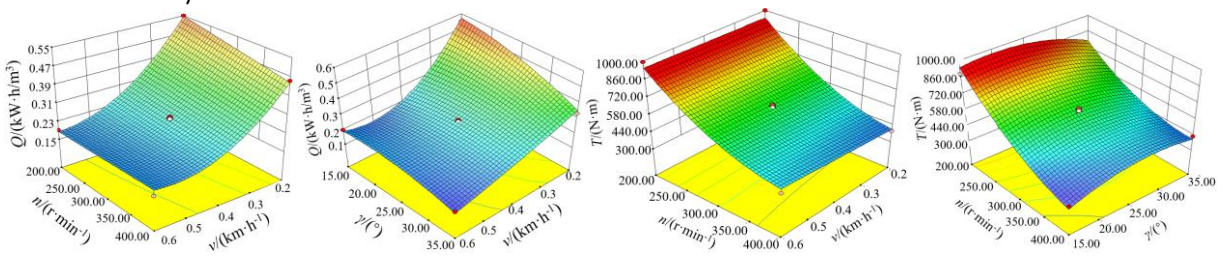

a) Impact of n and v on Q *b) Impact of γ and v on Q* *c) Impact of γ and v on T* *d)Impact of n and γ on T*

Fig. 10 - Response surfaces of T and Q under different *v*, *n*, and γ

Operation parameter optimization analysis

In the optimization process of reverse trencher operational parameters, a multi-objective optimization method was used to obtain the best parameter combination. The optimization equation can be expressed as follows:

$$\begin{cases} \min Q \\ \min T \\ 0.2 \le v \le 0.6 \\ 200 \le n \le 400 \\ 15^{\circ} \le \gamma \le 35^{\circ} \end{cases} \quad (8)$$

By solving the equation, the optimal speed v =0.29 km·h^{-1}, rotational speed n =394 r·min^{-1}, and angle γ=15° were found that minimize torque and specific energy consumption, achieving the best system performance. Subsequently, a coupled simulation test using the MBD-DEM method was performed with these optimal parameters. Under the optimal parameters, the mean torque and specific energy consumption were found to be 434.15 Nm and 0.321 kW·h m^{-3}, respectively.

Field validation test

Field tests were conducted in the vineyard of Shandong Gaomi Yifeng Machinery Co., Ltd. to validate the optimized operating parameters of the reverse trencher. During the tests, a torque sensor was used to connect the output shaft of the gearbox (with a reduction ratio of 1:4) to the trenching drive shaft, powered by the 12V battery of the tractor. The tractor's forward speed was adjusted to 0.29 km/h, and the working angle of the ditching machine was set to 15° by adjusting the hydraulic cylinder. The tractor's output shaft speed was 550 rpm (after the gearbox reduction, the speed was approximately 393 rpm). A data acquisition card was used to collect the voltage signals from the torque sensor at a sampling frequency of 20 Hz, converting these signals into torque values displayed on a computer. The operating scenario and results are shown in Fig.11.

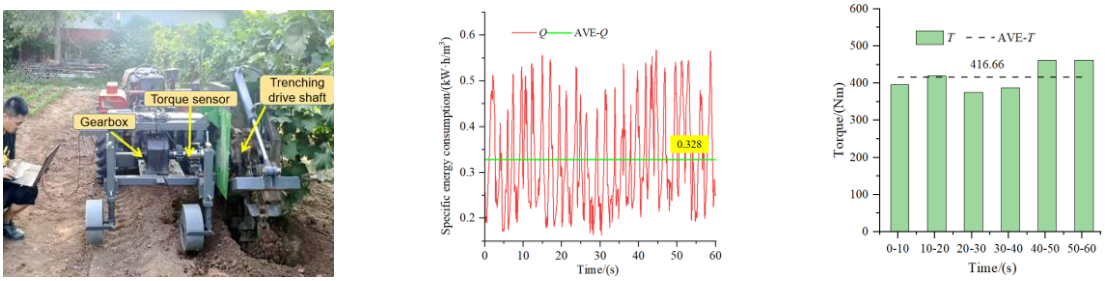

a) Testing process *b) Energy consumption results* *c) Torque results*

Fig. 11 - Field trial validation

The results of the field test show that under the optimized operating parameters, the energy consumption (Q) of the reverse trencher is 0.328 kW·h m^{-3}, with an error of 2.18% from the simulation results, and the mean torque is 416.66 Nm, with an error of 4.03% from the simulation results, which indicates that the operating parameters of the reverse trencher optimized on the basis of the test are accurate and reliable.

CONCLUSIONS

1. A reverse-rotating chain trencher was proposed, and a force analysis was conducted during the soil cutting and lifting stages of the device. The key operating parameters affecting trenching were identified as forward speed v, rotational speed n, and working angle γ. An MDB-DEM coupled simulation model of the trencher was established and simulated. Comparative analysis was performed on the characteristics of traditional trencher and the reverse trencher in terms of soil particle motion trajectories, velocities, and positions, demonstrating the feasibility of the reverse-rotating furrowing and backfilling scheme proposed in this study. A comparative analysis was conducted on the characteristics of traditional trenchers and reverse trenchers in terms of soil particle motion trajectories, velocities, and positions. The study demonstrated the feasibility of the reverse trencher scheme proposed.

2. The operating parameters of the reverse trencher was analyzed and optimized using the response surface method. Significant factors affecting mean torque and specific energy consumption were identified. Based on minimizing specific energy consumption and mean torque, multi-objective parameter optimization was conducted, determining the optimal operating parameter combination for the reverse trencher as follows: v=0.29 km h^{-1}, n=394 r min^{-1}, γ =15°. Simulating with these optimal parameters yielded a specific energy consumption of 0.321 kW·h m^{-3} and an average torque of 434.15 Nm under the optimal operating conditions.

3. To verify the accuracy of the simulation results, field tests were conducted with the optimal parameters. The field tests measured specific energy consumption and mean torque as 0.328 kW·h m^{-3} and 416.66 Nm, respectively, with errors of 2.18% and 4.03% compared to the simulation results. These relatively small errors validate the accuracy of the optimization results.

ACKNOWLEDGEMENT

This study was supported by the National Natural Science Foundation of China (32301710) and China Agriculture Research System of MOF and MARA (CARS-29).

REFERENCES

[1] Chen, W., Ren, J., Huang, W., Chen, L., Weng, W., Chen, C., Zheng S., (2024). Design and Parameter Optimization of a Dual-Disc Trenching Device for Ecological Tea Plantations. *Agriculture*, vol.14, pp.704, Fujian/China.

[2] Kešner, A., Chotěborský, R., Linda, M., Hromasová, M., Katinas, E., & Sutanto, H., (2021). Stress distribution on a soil tillage machine frame segment with a chisel shank simulated using discrete element and finite element methods and validate by experiment. *Biosystems Engineering*, vol.209, pp.125-138, Suchdol/Czech Republic.

[3] Liu, D., Gong, Y., Zhang, X., Yu, Q., Zhang, X., Chen, X., Wang Y., (2022). EDEM Simulation Study on the Performance of a Mechanized Ditching Device for Codonopsis Planting. *Agriculture*, vol.12, pp.1238, Xinjing/China.

[4] Liu, J., Jiang, P., Chen, J., Zhang, X., Xu, M., Huang, D., Shi Y., (2023). Optimal Design of and Experiment on a Dual-Spiral Ditcher for Orchards. *Agriculture*, vol.13, pp.1628, Hunan/China.

[5] Liu M., Xie F., Liu D., & Wang X., (2024). Analysis and Experiment on Power Consumption of Counter-rotating Ditcher Knife Roller Based on Particle Scaling Effect (基于颗粒放尺效应的逆旋开沟机刀辊功耗分析与试验). *Transactions of the Chinese Society of Agricultural Engineering*, vol.40, pp.83-92, Hunan/China.

[6] Ma, S., Niu, C., Yan, C., Tan, H., & Xu, L., (2021). Discrete element method optimisation of a scraper to remove soil from ridges formed to cold-proof grapevines. *Biosystems Engineering*, vol.210, pp.156-170, Beijing/China.

[7] Tamás, K., & Bernon, L., (2021). Role of particle shape and plant roots in the discrete element model of soil–sweep interaction. *Biosystems Engineering*, vol.211, pp.77-96, Hungary.

[8] Tan H., Ma S., Shen C., Ma J., Zhou H., Xu L., (2024). Development and Experiment of Organic Fertilizer Chain Reversing Ditching and Fertilizing Machine for Vineyard (葡萄园有机肥链式反转开沟施肥机研制与试验). *Transactions of the Chinese Society of Agricultural Engineering*, vol.40, pp.12-23, Beijing/China.

[9] Wang, J., Xu, Y., Wang, C., Xiang, Y., & Tang, H., (2023). Design and simulation of a trenching device for rice straw burial and trenching based on MBD-DEM. *Computers and Electronics in Agriculture*, vol.207, pp.107722, Harbin/China.

[10] Wang, L., Zhou, B., Wan, C., & Zhou, L., (2024). Structural parameter optimization of a furrow opener based on EDEM software. *International Journal of Agricultural and Biological Engineering*, vol.17, pp.115-120, Xinjiang/China.

[11] Wang, Y., Li, N., Ma, Y., Tong, J., Pfleging, W., & Sun, J., (2020). Field experiments evaluating a biomimetic shark-inspired (BioS) subsoiler for tillage resistance reduction. *Soil and Tillage Research*, vol.196, pp.104432, Jilin/China.

[12] Yang, Y., Hu, Z., Gu, F., & Ding, Q., (2023). Simulation and Experimental Study of the Tillage Mechanism for the Optimal Design of Wheat Rotary Strip–Tiller Blades. *Agriculture*, vol.13, pp.632, Beijing/China.

[13] Zeng Y., Jiang X., Wu M., Zhao Z., Tang L., & Li P., (2024). Development of layered cutting and throwing ditching cutter group based on DEM-MBD for Camellia oleifera forest (基于DEM-MBD的油茶林分层切抛式开沟刀组研制). *Transactions of the Chinese Society of Agricultural Engineering*, vol.40, pp.30-42, Hunan/China.